

Versatile Core–Sheath Yarn for Sustainable Biomechanical Energy Harvesting and Real-Time Human-Interactive Sensing

Kai Dong, Jianan Deng, Wenbo Ding, Aurelia C. Wang, Peihong Wang, Chaoyu Cheng, Yi-Cheng Wang, Limin Jin, Bohong Gu, Baozhong Sun, and Zhong Lin Wang*


The emergence of stretchable textile-based mechanical energy harvester and self-powered active sensor brings a new life for wearable functional electronics. However, single energy conversion mode and weak sensing capabilities have largely hindered their development. Here, in virtue of silver-coated nylon yarn and silicone rubber elastomer, a highly stretchable yarn-based triboelectric nanogenerator (TENG) with coaxial core–sheath and built-in spring-like spiral winding structures is designed for biomechanical energy harvesting and real-time human-interactive sensing. Based on the two advanced structural designs, the yarn-based TENG can effectively harvest or respond rapidly to omnifarious external mechanical stimuli, such as compressing, stretching, bending, and twisting. With these excellent performances, the yarn-based TENG can be used in a self-counting skipping rope, a self-powered gesture-recognizing glove, and a real-time golf scoring system. Furthermore, the yarn-based TENG can also be woven into a large-area energy-harvesting fabric, which is capable of lighting up light emitting diodes (LEDs), charging a commercial capacitor, powering a smart watch, and integrating the four operational modes of TENGs together. This work provides a new direction for textile-based multimode mechanical energy harvesters and highly sensitive self-powered motion sensors with potential applications in sustainable power supplies, self-powered wearable electronics, personalized motion/health monitoring, and real-time human-machine interactions.

1. Introduction

Modern electronics, which are indispensable for human health, safety, and communication, present a wide spectrum of opportunities to evolve our society into an intelligent world.^[1–3] To this end, considerable attention has been paid to wearable and flexible electronics, owing to their promising applications in a vast number of fields, ranging from flexible power supply,^[4–6] stretchable circuitries,^[7] personal healthcare/biomedical monitoring,^[8,9] artificial electronic skin,^[10,11] to wearable human-interactive interface.^[12] Among them, numerous types of self-powered functional sensors for health monitoring,^[13] motion tracking,^[14] medical care,^[15] personal protection, and security^[16] have been developed, which present an exciting opportunity to measure human physiology and mobility signals in a continuous, real-time, and noninvasive manner. However, the further advancement of wearable electronics still faces several critical challenges. First, the operations of these wearable electronics usually require external power sources. Conventional

Dr. K. Dong, Dr. J. Deng, Dr. W. Ding, A. C. Wang, Dr. P. Wang, C. Cheng, Dr. Y.-C. Wang, Prof. Z. L. Wang
School of Material Science and Engineering
Georgia Institute of Technology
Atlanta, GA 30332-0245, USA
E-mail: zhong.wang@mse.gatech.edu
Dr. K. Dong, Dr. L. Jin, Prof. B. Gu, Prof. B. Sun
College of Textiles
Key Laboratory of High Performance Fibers & Products
Ministry of Education
Donghua University
Shanghai 201020, P. R. China

Prof. Z. L. Wang
Beijing Institute of Nanoenergy and Nanosystems
Chinese Academy of Sciences
Beijing 100083, P. R. China
Prof. Z. L. Wang
College of Nanoscience and Technology
University of Chinese Academy of Sciences
Beijing 100049, P. R. China

 The ORCID identification number(s) for the author(s) of this article can be found under <https://doi.org/10.1002/aenm.201801114>.

DOI: 10.1002/aenm.201801114

power sources like electrochemical batteries suffer from heavy weight, bulky volume, and limited capacity and lifetime, largely hindering the practical and sustainable use of wearable electronics.^[17,18] Second, conventional planar structure has limited wearable development, due to large deformations of the human body in motion that may degrade or even damage the structure and function of wearable electronics². Third, it is difficult to achieve an electrode that possesses high stretchability while maintaining excellent electrical conductivity, since the electrical conductivities of most electrode materials, such as, carbon nanotubes/nanofibers,^[19,20] graphene,^[20–22] metal nanowires/nanotroughs,^[20,23] and conductive polymers,^[24,25] decline sharply or even disappear at high tensile state. Last but not least, the current self-powered wearable sensors typically target a single type of human movement.^[18,26,27] Preferably, wearable sensors should be able to respond to multiple forms of mechanical stimuli, such as stretching, compressing, bending, and twisting, in an efficient, timely, and sensitive way. The existence of these factors restricts the applications and scopes of wearable energy harvesters and self-powered functional sensors.

In order to provide a continuous, self-sufficient, and sustained power for wearable electronics, the newly developed triboelectric nanogenerator (TENG) is an energy-harvesting technology that can convert ubiquitous mechanical energy into electricity based on a coupled effect of contact-electrification and electrostatic induction.^[18,28–30] Due to its high efficiency, light-weight, low-cost, environmental friendliness, and universal availability, it has promising applications both in scavenging small mechanical energy and large-scale energy generation. The TENG has been demonstrated to harvest different types of mechanical energies that are omnipresent but otherwise wasted in our daily life, such as human motion,^[31] mechanical triggering,^[32] vibration,^[33] wind,^[34] flowing water,^[35] and more. In addition, a TENG can also be used as a self-powered sensor to actively detect the static and dynamic processes arising from mechanical movements through monitoring its real-time voltage or current signals,^[27,31,36] which has potential applications in real-time human-interactive sensing systems. The integration of TENG technology into traditional textiles brings more possibilities for wearable electronic textiles as well as self-powered sensing devices.^[31,37–39] Textile-based TENGs are highly desirable for next-generation energy harvesters and self-powered sensors that are expected to be lightweight, long-lasting, breathable, deformable, and washable. This new class of wearable electronics can conform into complex, nonplanar shapes while maintaining satisfactory performance, reliability, and integration.

Herein, a novel and multifunctional core–sheath yarn-based TENG is designed and fabricated, in which an internal core column is axially inserted into an external sheath tube. Due to the built-in spring-like and core–sheath conjugate structures, the developed yarn-based TENG is flexible, stretchable, conformable, long-lasting, and highly sensitive to a variety of mechanical stimuli, aiming at scavenging versatile biomechanical energies as well as capturing various types of human motion signals. In order to exhibit its superior performance, a self-counting skipping rope, a self-powered smart gesture-recognizing glove, and a real-time golf scoring system are introduced and demonstrated successively in this paper. Finally, a

large-area energy-harvesting fabric based on the yarn-based TENG is fabricated to investigate its capabilities in lighting up light emitting diodes (LEDs), sustainably charging commercial capacitors, and driving a digital watch. Furthermore, through adjusting circuit connection modes and external load imposing methods, the fabric can integrate the four operational modes of TENGs together, further demonstrating its diverse energy-harvesting capabilities. The present work contributes a wide variety of applications of textile-based TENGs with diverse energy-harvesting methods and real-time self-powered human-interactive sensing systems, which will lead wearable electronics toward a more intelligent, more convenient/accessible, and more environmental friendly development direction.

2. Results and Discussion

It is generally believed that after two different materials come into contact with each other, a chemical bond is formed between the two surfaces and charges move from one material to the other to equalize their electrochemical potential.^[18,28,29,40] The transferred charges will drive free electrons to flow back and forth to screen the induced potential difference between the two materials. In this way, the applied mechanical energy is converted into electricity. Therefore, selection of the appropriate paired tribomaterials with opposite triboelectric polarities from the triboelectric series is crucial to achieve an enhanced electrical output TENG. In addition to the material itself, the organizational structure of a TENG is also very important for its overall performance. As we know, adequate space for contact separation operation is essential for a TENG. Furthermore, specialized structural design is prerequisite for achieving excellent dynamic and mechanical properties in a TENG. Taking all these factors into account, we designed a highly stretchable core–sheath structural yarn-based TENG with diverse mechanical energy conversing modes and excellent mechanical stability (**Figure 1**).

Conductive fibers are an attractive platform for flexible and stretchable electronics because fibers are inexpensive, inherently flexible, can be formed into 2D and 3D fabrics, and can be mass produced. In the present work, 3-ply-twisted silver-coated nylon yarn (nominal diameter: 180 μm , resistance $<100 \Omega \text{ cm}^{-1}$, Figure S1a,b, Supporting Information) is selected as the electrode material due to its excellent electrical conductivity, mechanical robustness, and easy accessibility. Supersoft yet tough silicone rubber is chosen as the dielectric, supporting, and encapsulating material owing to its good biocompatibility, superior mechanical properties, excellent flexibility/stretchability, and strong tendency to gain electrons. According to its fabrication process in Figure 1a, the yarn-based TENG consists of two parts: an internal core column and an external sheath tube, both of which present a spring-like spiral winding structure. This special spiral winding structure is obtained based on outer rotation and torque loading, as illustrated in Figure S2 and further discussed in Note S1 in the Supporting Information. As the surface morphology scanning electron microscopy (SEM) shows in Figure 1b (middle), the internal core column is fabricated with a conductive nylon yarn (as an inner electrode) winding in a spiral around a pure silicone rubber fiber column (as a support). A commercial elastic silicone rubber tube was

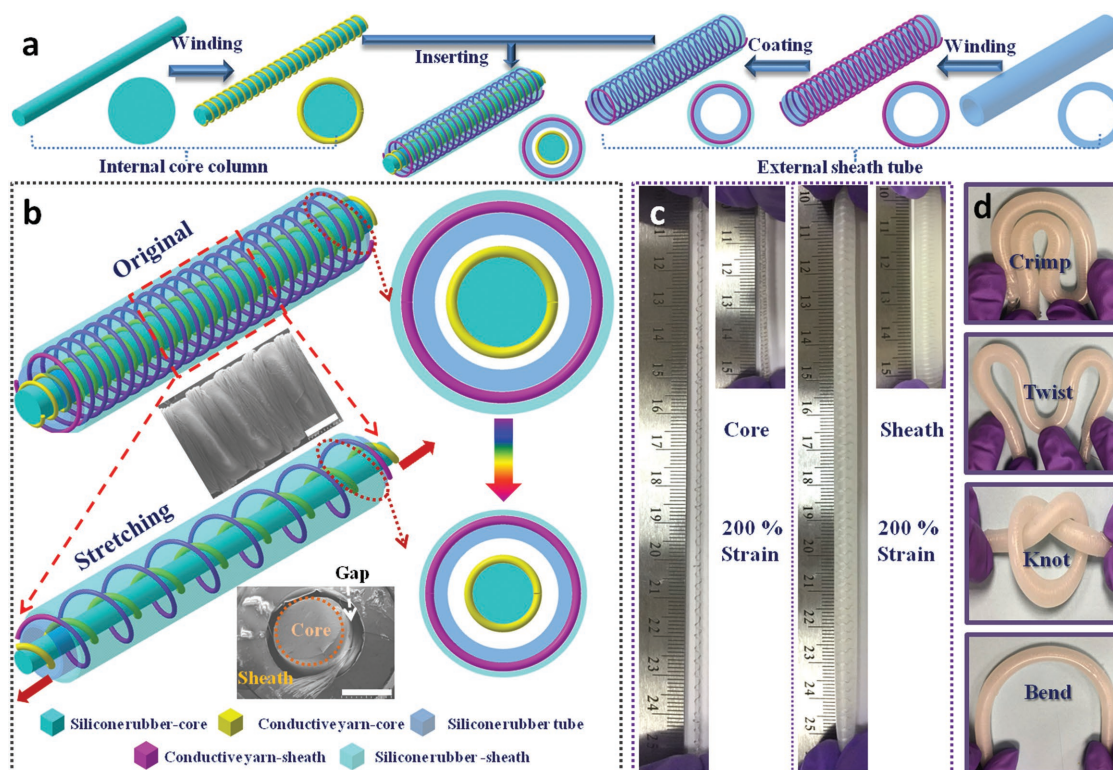


Figure 1. Schematic illustration, fabrication process, and mechanical behavior of the yarn-based TENG. a) Fabrication process of the coaxial core–sheath yarn-based TENG. b) Schematic diagrams of the yarn-based TENG before and after stretching. The inserted SEM images are the surface morphology of the spring-like spiral winding structural internal core column (middle), and the cross section of the yarn-based TENG (lower right). c) Photographs demonstrating the excellent tensile behaviors of the internal core column and the external sheath tube (200% tensile strain). d) Photographs of the yarn-based TENG with demonstrations of being subject to different mechanical forces, including crimping, twisting, knotting, and bending.

chosen as the framework to form the external sheath tube, whose surface was twisted on another conductive nylon yarn (as an outer electrode) and encapsulated by another layer of silicone rubber solution (as encapsulating material). After the internal core column is axially inserted into the external sheath tube, a coaxial core–sheath yarn-based TENG with a built-in spring-like structure can be fabricated, whose cross-section SEM images are shown in Figure 1b (bottom) and Figure S1c,d (Supporting Information). A more detailed description of the fabrication method is mentioned in the “Experimental Section.” Due to the spring-like spiral winding structure, both the internal core column and the external sheath tube exhibit high stretchability (up to 200% tensile strain, Figure 1c). As a combination of the two, the as-produced yarn-based TENG also presents high stretchability (Figure 1b). To further investigate the stretchability of the yarn-based TENG, its stress–strain behaviors are also traced under various tensile strains (Figure S3, Supporting Information). In addition to the excellent stretchability, the yarn-based TENG can also sustain other kinds of complex mechanical deformations, such as crimping, bending, knotting, and twisting (Figure 1d), further demonstrating its promising applications in wearable electronics as well as self-powered sensing devices.

As indicated above, our TENG can work under various kinds of mechanical stimuli. However, the electricity generating mechanisms behind these external loadings are nearly the same, which is based on the coupling of contact electrification and

electrostatic induction.^[18,28–30] Herein, only the working principle of the stretching operation is discussed. For a better and more intuitive understanding of the charge transfer process during the contact separation movement, two kinds of sections (i.e., parallel to or perpendicular to the yarn’s axial direction) are demonstrated (Figure 2a). The whole stretching–releasing motion in a cycle can be simplified as one contact–separation process that occurs between the inner conductive yarn and the middle silicone rubber tube. In the original stage (Figure 2ai), the internal core column partially contacts with the middle silicone rubber tube due to gravity. The middle silicone rubber tube is proven to be negatively charged because of its ability to attract more electrons than the silver. No charge transfer appears on either side at this state because of the absence of electrical potential differences. When the device is stretched along its axial direction, both the internal core column and the external sheath tube elongate axially while contracting radially (Figure 2aaii). Due to different Young’s modulus, the internal core column will gradually separate from the external sheath tube. This process results in induced positive charges accumulating in the outer yarn electrode due to the electrostatic induction. Consequently, free electrons in the outer yarn electrode will flow into the inner yarn electrode to balance the electrostatic status, which thereby generates an instantaneous positive current. As the tensile distance reaches its maximum, the internal core column is fully separated with the external sheath tube (Figure 2aaiii). Both the electrical potential of the inner yarn

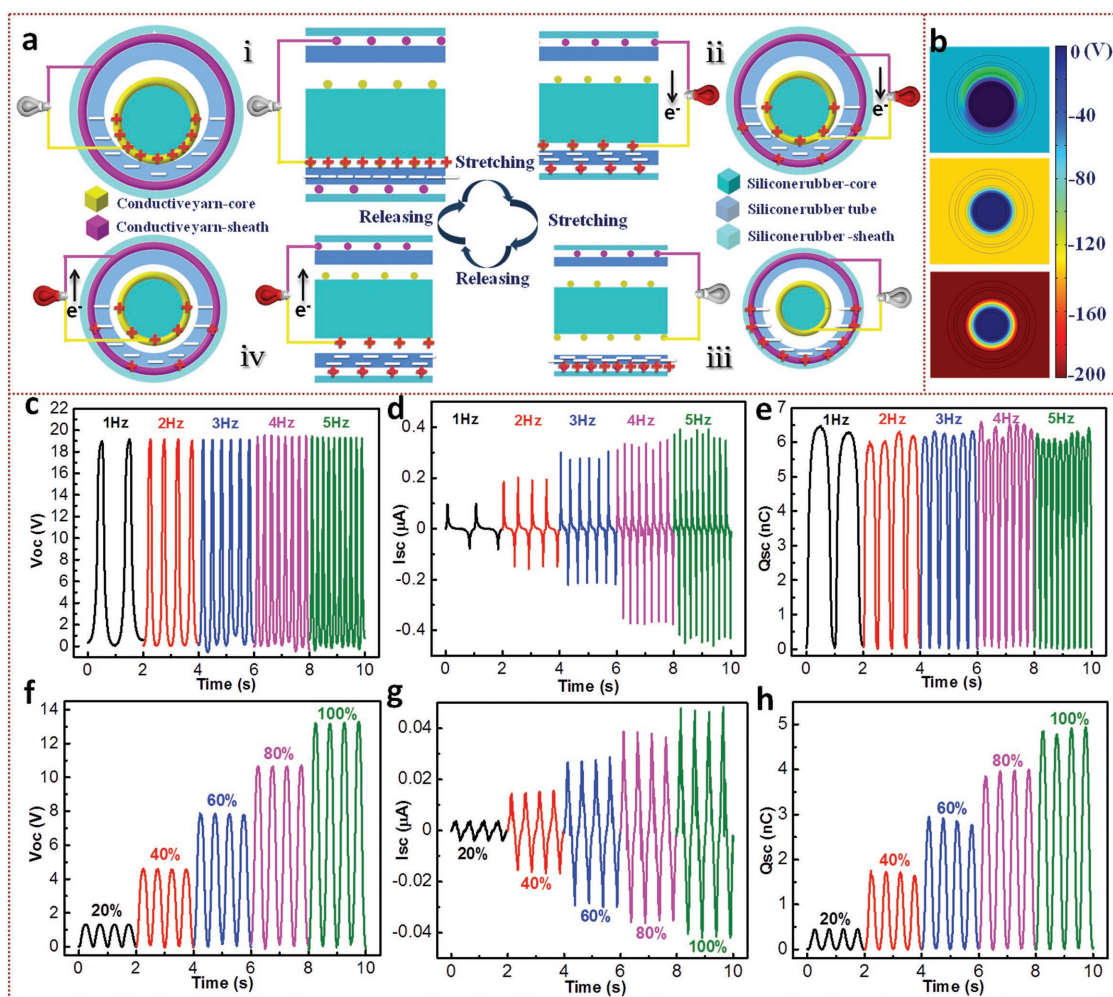


Figure 2. Working mechanism and electrical output performance of the yarn-based TENG. a) Schematic diagram of the working principle of the yarn-based TENG under the stretching state. Two kinds of sections that parallel to and perpendicular to the yarn's axial direction are selected. b) Simulation of the potential distribution of the yarn-based TENG under open circuit condition by using COMSOL software. Electrical outputs of the yarn-based TENG under various compressing frequencies (1–5 Hz), which include c) V_{OC} , d) I_{SC} , and e) Q_{SC} (contact length: 20 mm, and compressing force: 20 N). f–h) Electrical outputs of the yarn-based TENG under various tensile strains (20–100%), including f) V_{OC} , g) I_{SC} , and h) Q_{SC} (initial clapping length: 30 mm, and stretching frequency: 2 Hz).

electrode and the amount of transferred charges reach their maximum values at this point. There is an absence of electrical signal in this electrical equilibrium state, which reflects the neutralization of both positive and negative charges. It is necessary to note that the transferred and accumulated charges on the middle silicone rubber tube will not be entirely annihilated, even when the two triboelectric layers are subsequently separated. Instead, the electrostatic charges will be maintained for a sufficiently long time because they have been naturally impregnated into the insulator silicone rubber. In the reverse case, when the device is released (Figure 2aiv), the electrical potential of the inner yarn electrode drops and electrons flow back to the outer yarn electrode from the inner yarn electrode through the external load. After the whole system recovers back to its original state (Figure 2ai), the negative charges on the middle silicone rubber tube are fully offset by the positive charges on the inner yarn electrode again. As a result, a contact-separation process between the internal core column and the external

sheath tube will generate an instantaneous alternating potential and current through the load. The observations of the electrostatic potential distributions of every component at stretching state and releasing state are realized by using COMSOL Multiphysics, as illustrated in Figure 2b and Figure S4 (Supporting Information).

Diverse working modes endow our yarn-based TENG with a variety of energy-harvesting methods. The electrical output performances of the yarn-based TENG, including open-circuit (OC) voltage (V_{OC}), short-circuit (SC) current (I_{SC}), and short-circuit (SC) charge transfer (Q_{SC}), are measured and analyzed under each loading state, respectively. In the current work, we mainly use a linear motor to impose these mechanical loadings, such as compressing, stretching, and bending (Figure S5 and Movie S1, Supporting Information). Before conducting the corresponding measurements, the circuit connection modes are first investigated. As shown in Figure S6a (Supporting Information), there are almost four kinds of circuit connection modes

existing in the yarn-based TENG, that is, the inner electrode connecting with the outer electrode, series-connected inner and outer electrodes connecting to the ground, only the outer electrode connecting to the ground, and only the inner electrode connecting to the ground. According to their compression-induced electrical output performances shown in Figure S6b (Supporting Information), it is obvious that the inner electrode connecting with the outer electrode is the optimal circuit connection mode for the yarn-based TENG. In the following investigations, only this kind of circuit connection mode is studied and reported. Under different compressing frequencies (1–5 Hz), the V_{OC} and Q_{SC} almost remain constant (19 V and 6.5 nC, respectively). However, the I_{SC} increases from 0.1 to 0.43 μA , revealing a clearly enhanced trend with the increase of frequency (Figure 2c–e). In other words, the increase in frequency is favorable for the magnitude of I_{SC} . Under higher frequency, the higher deformation rate leads to a higher flow rate of charges between two triboelectric layers, resulting in a higher current generation. The similar electrical output trends can be also observed in the stretching process. At a fixed tensile strain of 100%, the V_{OC} and Q_{SC} are basically stabilized at 13.5 V and 5 nC, respectively, while the I_{SC} increases from 0.03 to 0.1 μA (Figure S7, Supporting Information). When the yarn-based TENG is stretched under various tensile strains, its compression-induced electrical output performance gradually degrades with the increase of tensile strain (Figure S8, Supporting Information). Due to the increase of tensile strain, the yarn gradually shrinks in the radial direction, resulting in a decreased contact area with the active layer. The effect of tensile strain on the electrical outputs of yarn-based TENG is also investigated, as shown in Figure 2f–h. At a fixed stretching frequency of 2 Hz, its electrical outputs almost linearly increase with the increment of tensile strain (20–100%). As tensile strain increases, more adequate separation between the internal core column and the external sheath tube will be achieved, contributing to greater released contact area. The electrical output performance of the yarn-based TENG under bending and stretching–bending coupled states is also investigated, which also exhibits an increased trend with the increase of loading strain (Figure S9, Supporting Information). In addition to compression, stretching, and bending, the yarn-based TENG also shows a favorable electrical output performance under a hand twisting state (Figure S10, Supporting Information). To further reveal the relationship between the external mechanical loadings and electrical output performance, a wide range of applied forces are imposed. As illustrated in Figure S11 (Supporting Information), the electrical output gradually increases with the increase of compression or tensile forces, demonstrating the highly stress sensitivity of our yarn-based TENG. The excellent electrical output performance and highly stress sensitivity of the yarn-based TENG are attributed to its built-in spring-like spiral winding and core–sheath structures. Among them, the gap existing between the internal core column and the external sheath tube plays a key role. As shown in Figure S12 (Supporting Information), the electrical output measurements with a gap are significantly higher than those without a gap, further verifying that the gap is an indispensable part of the yarn-based TENG. The ability to perceive small strain variations enables our yarn-based TENG to be used as a microforce sensor, which shows a promising application in

high sensitive human-machine interactions. To characterize the power output performance of our yarn-based TENG, external variable resistors (10 k Ω to 3 G Ω) are connected in series in the circuit. As shown in Figure S13 (Supporting Information), the average output currents first remain at the maximum value and then decrease sharply with the increment of resistances from 10 M Ω to 3 G Ω . The instantaneous average volume power densities of a single yarn-based TENG reach peak values of 11 and 0.88 W m $^{-3}$ under the compression state and tensile state, respectively. The average power densities of the yarn-based TENG are calculated as I^2R/V , where I is the output current across the external load, and R is the load resistance. V represents the volume of the yarn-based TENG and can be calculated as πr^2L , where r refers to the outermost radius of the circular TENG yarn, and L is the compression sample length or initial tensile clamping length. The energy conversion efficiency of the yarn-based TENG is defined as the ratio between the input mechanical energy and the generated electrical energy. The detailed calculation method of the energy conversion efficiency is investigated in Note S2 (Supporting Information). Under the compression state, the established total energy conversion efficiencies under different resistances from a number of repeated measurements are shown in Figure S14 (Supporting Information). It can be observed that the highest efficiency reaches nearly 20% at an external load of 700 M Ω . The long-term stability and durability of the yarn-based TENG are also investigated both at compression and tensile states. As shown in Figure S15 (Supporting Information), almost no significant decreases of I_{SC} are found even after 50 thousand continuous loading cycles, clearly demonstrating the practical value of this stable and reliable energy-harvesting yarn.

On the basis of the strong advantages of the yarn-based TENG demonstrated above, we first develop a self-counting skipping rope, which consists of three parts: a bottom touchdown section, two middle connection sections, and two hand holding sections (Figure 3a). The skipping rope's digital photograph and practical operating status are demonstrated in Figure 3b,c, respectively. The fabrication method of this self-counting skipping rope is introduced in the "Experimental Section." The hand holding section requires a certain stretchability and excellent mechanical stability, which coincides with the basic properties of the as-prepared yarn-based TENG. Therefore, two yarn-based TENGs are placed in the hand holding sections as handles. The counting signal of skipping rope stems from the contact-separation motions between the bottom touchdown section and the ground (Figure 3d). In order to increase the electrical output of the bottom touchdown section as well as enhance its mechanical strength, a double-coated structure is designed by coating an inner silicone rubber layer on a core conductive yarn, and then spirally winding an outer conductive yarn, and finally coating with an outer silicone rubber layer (lower right in Figure 3a, top right and lower right in Figure 3d). The middle connection section, acting as a connection medium and support, plays a role in transmitting electrical signals, which also requires good electrical conductivity and modest mechanical strength. The core conductive yarn from the bottom touchdown section runs through the two middle connection sections, spirally wound by the outer conductive yarn from the bottom touchdown section, and finally coated

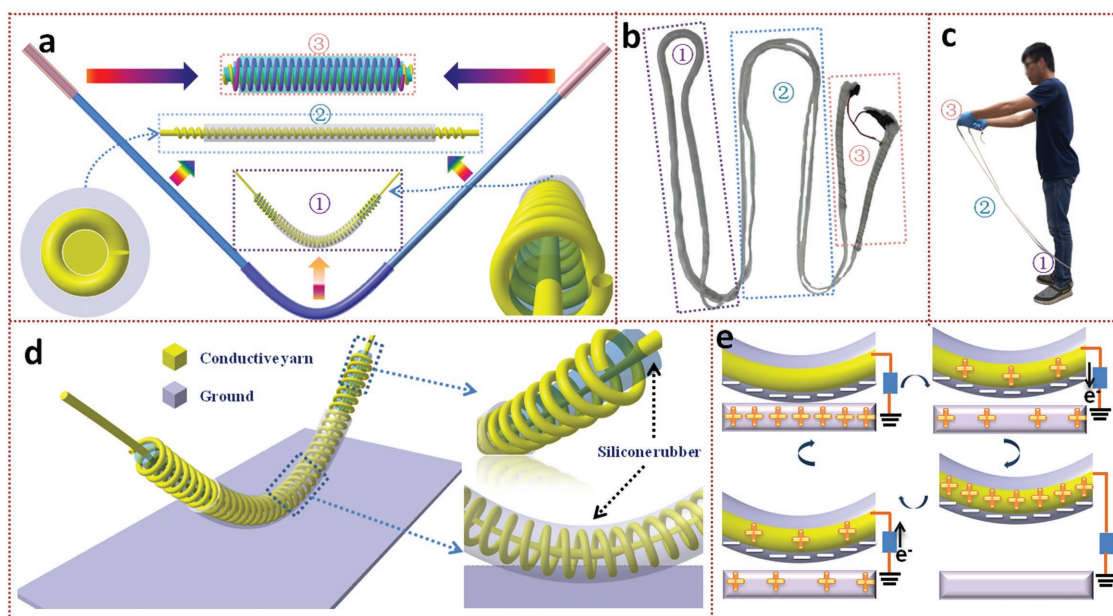


Figure 3. Application of the yarn-based TENG as a self-counting skipping rope. a) Schematic illustration of the self-counting skipping rope, which mainly includes three parts: a bottom touchdown section (1), two middle connection sections (2), and two hand holding sections (3). The insets are the cross section of the middle connection section (lower left) and the side 3D view of the bottom touchdown section (lower right). b) Photograph of the as-prepared self-counting skipping rope with the three components marked. c) Photograph demonstrating the actual operation state of the skipping rope. d) Schematic structure of the bottom touchdown section. e) Working mechanism of the self-counting skipping rope.

by the outer silicone rubber (lower left in Figure 3a). Through these designs, a high sensitive, flexible, soft-yet-robust self-counting skipping rope is developed. The working mechanism of this self-counting skipping rope is described as a single-electrical mode TENG (Figure 3e). Rope skipping one time is one contact-separation process between the skipping rope and the ground, which will generate an instantaneous alternating current signal. The collected current signals (Figure S16a, Supporting Information) are further transferred to the data analysis system to distinguish their amplitudes. Only signal that exceeds a certain threshold is considered to be one skip count. The real-time self-powered rope skipping automatic counting system is demonstrated in Movie S2 (Supporting Information), which performs an accurate and fast measurement. The software output interface and actual operation environment are also shown in Figure S16b,c (Supporting Information), respectively. The developed self-counting skipping rope not only provides more options for future automatic counting systems but also broadens the application scenarios of the self-powered human-interactive systems.

In virtue of its highly sensitivity to diverse external mechanical stimuli, our yarn-based TENG can be further designed as a self-powered smart gesture-recognizing glove, which is readily achieved by fixing five TENG yarns on the dorsal side of a regular glove with kapton tape (Figure 4a). It is necessary to point out that each TENG yarn is connected with an external resistor ($2\text{ G}\Omega$) for keeping output voltage stable as well as avoiding the damage of high voltage to the data acquisition system, whose rated voltage is 10 V. As mentioned above, the bending strain, or in other words the bending angle, affecting the electrical output performance of the TENG yarn, is the main reason for the electrical output differences among the five fingers

(i.e., thumb, index, middle, ring, and little finger), which is also discussed in detail (Figure S15, Supporting Information). By sewing a TENG yarn on the index finger of a glove, the relationship between the bending angles and the electrical output performance is investigated (Figure S17a, Supporting Information). As the index finger is slowly and repeatedly bended and relaxed, the real-time OC voltage output shows a gradual and periodic synchronous increase and decrease, demonstrating real-time self-powered finger motion detection (Movie S3, Supporting Information). In addition, it is also obvious that the electrical outputs of this TENG yarn increase with the higher bending angles (Figure S17b,c, Supporting Information), further verifying its feasibility for use in recognition of different gestures. The voltage output signals of the five fingers are collected by bending them in turn from the thumb to the little finger, as shown in Figure 4b. It is worth noting that when a finger is bent, other fingers will also have slight resonant reactions. However, the voltages of the finger at the bending state are significantly higher than those at the motionless states, indicating that the interference signals from the motionless fingers can be effectively distinguished. When a finger is bent, its real-time voltage signal will be collected by the data acquisition system and transmitted to the computer. After data processing, analyzing, and matching, the indicator on the corresponding finger will be lit up in the software output window, when the voltage signal of one finger reaches its precollected signal range. For example, the indicators of the thumb and ring finger turn green when they are bent (Figure 4c). The software output window is shown in Figure 4d, including a gesture recognition indicator and a real-time voltage output interface. According to the instructions, the hand can conduct a series of movements, such as wiggling fingers in sequence (from thumb

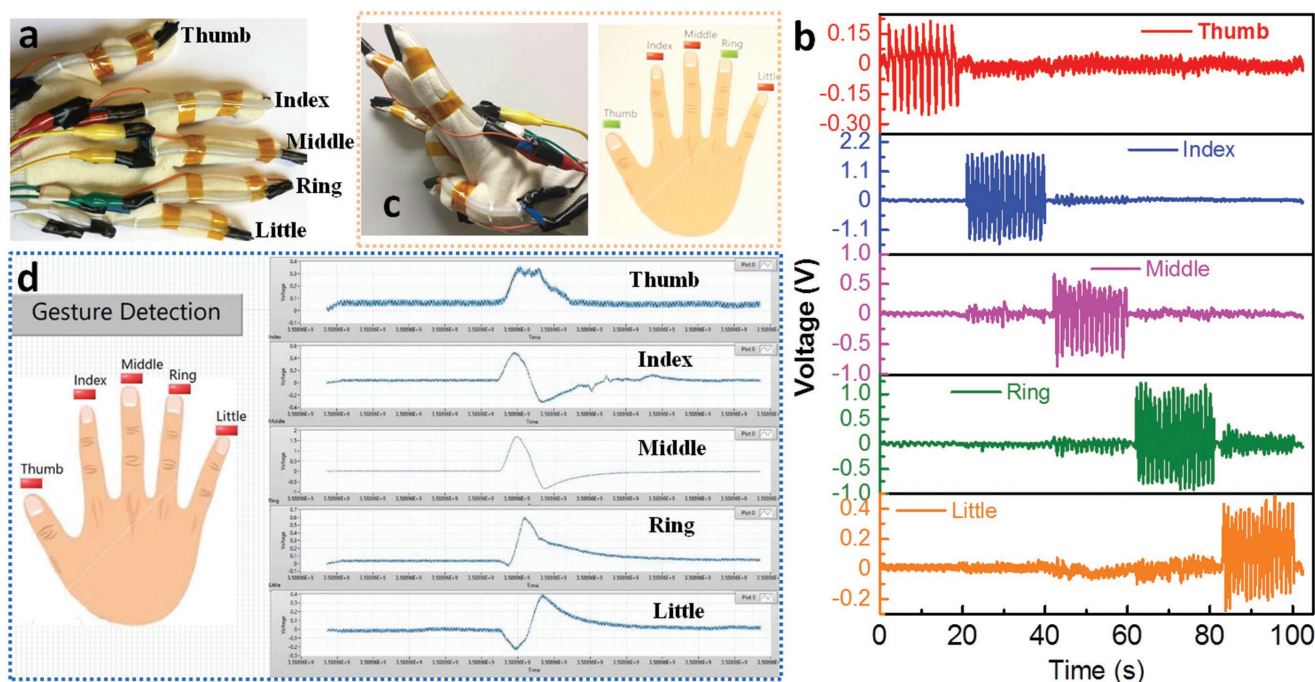


Figure 4. Application of the yarn-based TENG in a smart glove for gesture detection and recognition. a) Photograph of the smart glove with the yarn-based TENGs fixed on its dorsal side. b) Voltage output signals of the five fingers by wiggling them from the thumb to the little finger in turn. c) Photograph demonstrating the operating mode of the gesture-recognizing glove. When the fingers are wiggling, the corresponding indicators on the software output interface will be lit up. d) Photograph of the software output interface for real-time gesture detection and recognition.

to little finger), wiggling one finger at a time, wiggling two fingers at a time, and wiggling fingers together, which are demonstrated in Movie S4 (Supporting Information). In short, our self-powered smart glove can detect human gesture transformations in a real-time, fast, and convenient manner, which has promising applications in multifunctional motion sensors and user-friendly health monitoring.

Thanks to its highly sensitivity and versatile energy conversion modes, our yarn-based TENG not only can recognize simple, one-time motion signals as mentioned above but can also continuously capture a period of complex movements. It is well known that converting a series of standard actions into continuous electrical signals is very useful and convenient for trainers to master the skills and operation specifications of a sports event more efficiently. A good golf swing is crucial to achieving adequate control over the ball and a successful score. Here, to provide guidance for playing golf, a real-time and self-powered golf scoring system is developed and implemented, which consists of two proposed yarn-based TENGs, a voltage measurement device, a data acquisition system, and the specially developed data analysis and scoring software (Figure 5a). The two yarn-based TENGs are sewn on the arm lateral and medial of a sleeve, respectively, to monitor the action standard of a golf swing through detection of their electrical signals. Similar to the above smart glove, the two yarn-based TENGs are also connected with an external resistance of $1\text{ G}\Omega$, respectively. As illustrated in Figure S18 (Supporting Information), the yarn fixed on the arm lateral withstands the stretching and bending coupled stimuli, while the one on the arm medial is subjected to the compressing and bending dual deformations. The different

deformation modes between them lead to their different electrical output performance. A complete golf swing standard action is split up into eight motion processes for better understanding the relationship between the arm swing movements and the voltage output signals (Figure 5b). First, a golfer holds a golf club by the grip with both hands (1), and then brings the club up and around himself to set up a good strong swing (2). Afterward, he swings the club around and toward the golf ball (3). After striking the golf ball, the arm completes the swing and will continue to rise up due to inertia (4), until it reaches the maximum bending state (5). Then, the retracting arm action will begin by bringing the club down (6), gradually straightening the bent arm (7), and finally returning to the initial position (8). After repeating these actions, the real-time voltage signals of the two yarn-based TENGs are collected (Figure 5c), which show a good repeatability and continuity. Furthermore, a complete curve of a golf swing is selected and further divided into eight short periods (Figure 5d), which corresponds to the eight fore-mentioned motion processes (Figure 5b). It can be found that the instantaneous action is converted to the corresponding electrical signal in a real-time and convenient way, demonstrating its great advantages in real-time human-machine interactions. The generated voltage signals are collected by a data acquisition system and further transmitted to the data analysis and scoring software for similarity comparison. After the conformance analysis with the preacquired voltage signals of standard actions, the final score and grade evaluation are obtained. According to the assessed scores (maximum score is 100), there are four levels (i.e., fail, good, very good, and excellent) possible to evaluate the action standard. As demonstrated in Movie S5

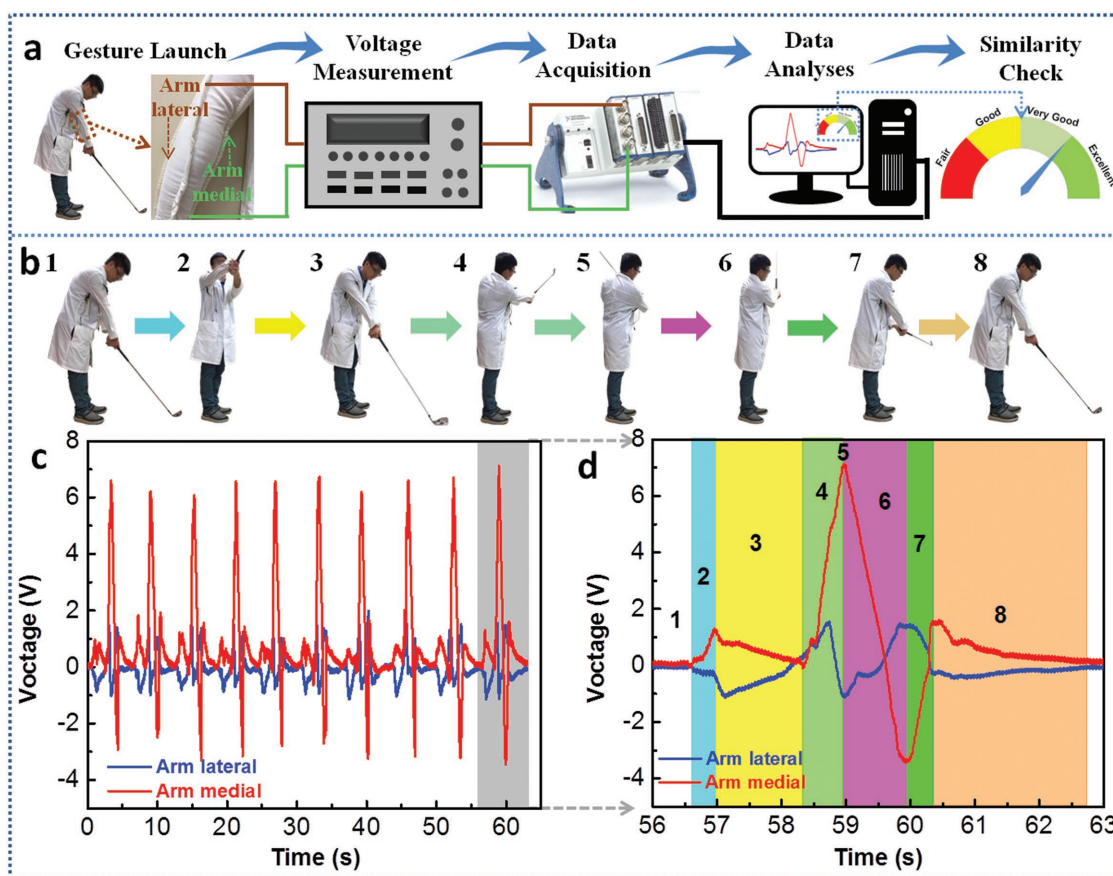


Figure 5. Application of the yarn-based TENG in a real-time golf scoring system. a) Technique route of the real-time golf scoring system, which consists of two proposed yarn-based TENGs, a voltage measurement device, a data acquisition system, and the specialized developed data analysis and scoring software. The two yarn-based TENGs are sewn on the arm medial and lateral of a sleeve, respectively. b) Eight consecutive snapshots selected from the complete set of a golf swing action. c) Real-time voltage output signals of the two yarn-based TENGs collected in the process of performing golf swings. d) An amplified voltage signal of the two yarn-based TENGs in a complete golf swing process. The voltage curve can be divided into the eight sections corresponding to the eight golf swing steps in panel (b).

(Supporting Information), the real-time golf scoring system can quickly and adequately evaluate the features and success of a golf swing, which will lead future human-interactive motion sensing and monitoring applications to evolve into a deeper and broader field.

In addition to the multifunctional sensing applications, our yarn-based TENG can also be woven into a large-area energy-harvesting fabric for more extensive applications in wearable electronics. As shown in **Figure 6a,b**, a large-area energy-harvesting fabric is fabricated by interlacing the parallel-arranged TENG yarns with acrylic yarns into a plain woven pattern. Moreover, a multimode energy-harvesting fabric (**Figure 6c**) is also designed by mutually crosswise arranging the energy-harvesting yarns and acrylic yarns in the weft direction, and then interweaving with polyester yarns, in which the acrylic yarns play a role in separating the adjacent electrodes. As we know, there are generally four types of working modes for a TENG, i.e., single electrode mode, contact-separation mode, sliding mode, and freestanding mode.^[18,28,29,40] Through altering the external force imposing method and the circuit connection mode, we can integrate the four working modes together. By wearing the multimode energy-harvesting fabric on an

individual's arm, 23 series-connected flower-shaped LEDs can easily be lit up by hand flapping (**Figure 6d**; **Movie S6**, Supporting Information). Furthermore, with the help of full-wave bridge rectifiers, the converted electricity from human body movements can be stored in a capacitor or battery for later use. A commercial capacitor with the storage capacitance of 1 μF can be charged to 3.5 V after about 7 s through hand flapping against the fabric (**Figure 6e**; **Movie S7**, Supporting Information). In addition, through designing an appropriate circuit diagram (**Figure S19**, Supporting Information), the storage electricity can sustainably drive an electronic watch (**Figure 6f**; **Movie S8**, Supporting Information), which shows its practical application value in our daily life. The detailed introductions of the multimode energy-harvesting fabric under the four working modes are also exhibited in **Figure 6g–j**. In each energy-harvesting mode, there is a corresponding load imposing way (**Figure 6g**) and circuit connection mode (**Figure 6h**). For the single-electrode mode with all sheath electrodes connecting to the ground (**Figure 6h12**), there is a clear separation distance between an active object (a hand in this case) and the fabric (**Figure 6h11**). However, in the contact-separation mode, the hand contacts with the fabric firmly with all the sheath

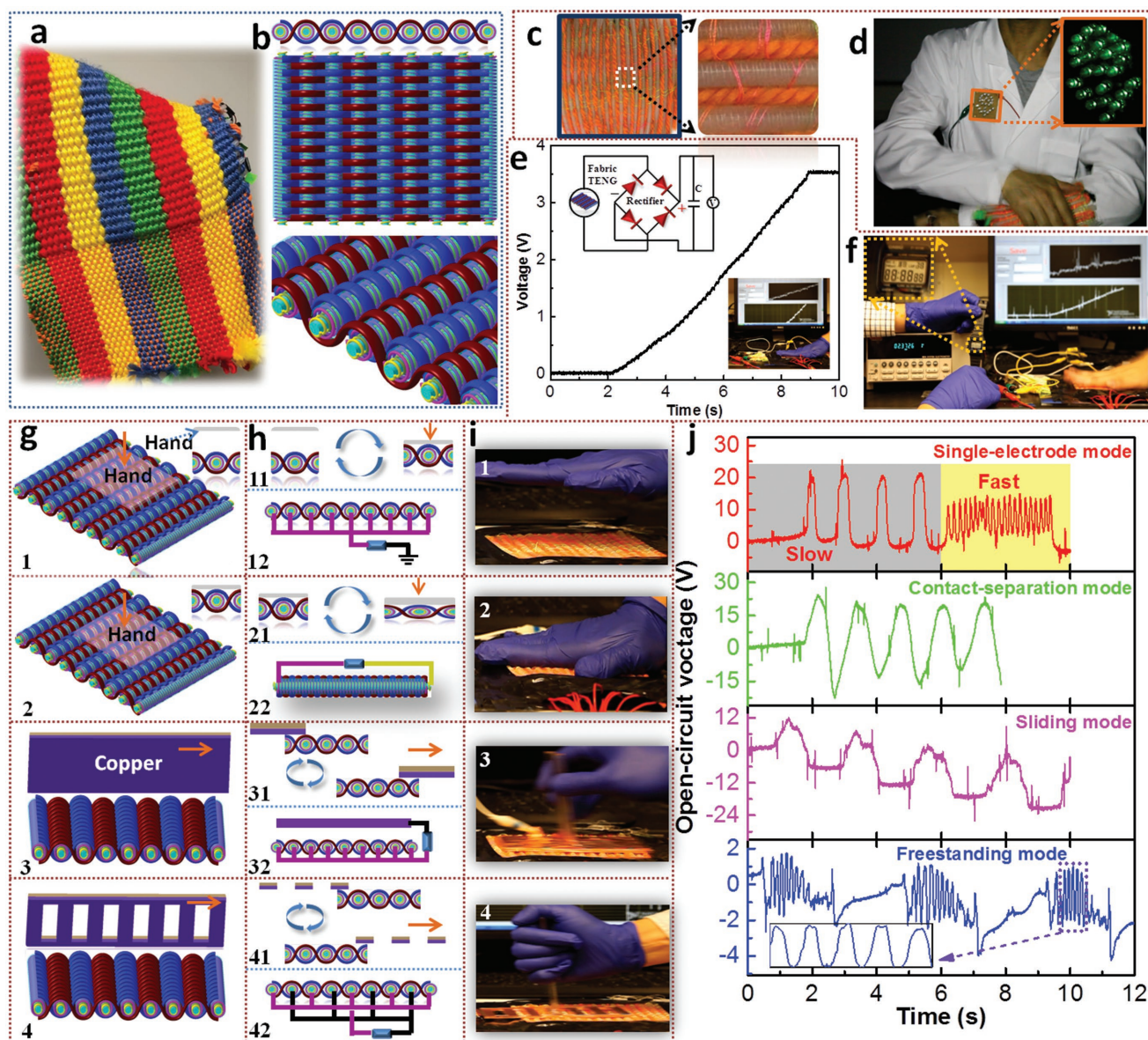


Figure 6. Digital photograph, schematic diagram, and application demonstration of large-area energy-harvesting fabrics. a) Photograph of a large-area energy-harvesting fabric. b) Schematic illustration of this fabric. The top, middle, and bottom are the side, vertical, and partial enlarged 3D views of the fabric, respectively. c) Photograph of a multimode energy-harvesting fabric that can integrate the four operational modes of TENGs together. d) Photograph demonstrating that the multimode energy-harvesting fabric can easily light up 23 flower-shaped LEDs just by using a palm to flap it. e) Charging capability of the multimode energy-harvesting fabric by hand flapping. The circuit diagram and charging process are also inserted its top left and lower right, respectively. f) Demonstration of continuously driving a smart watch by hand flapping this fabric. g) Schematic illustration exhibiting the external load imposing methods of the four working modes. And 1, 2, 3, and 4 represent the single-electrode, the contact-separation, the sliding, and the freestanding modes, respectively. The orange arrow represents the external load applied direction. h) Schematic diagram showing the contact-separation movements (11, 21, 31, and 41) and electrical connection methods (12, 22, 32, and 42) of the multimode energy-harvesting fabric under different working modes. i) Photograph demonstrating the practical load imposing methods of the multimode energy-harvesting fabric under different working modes. j) OC voltage outputs of multimode energy-harvesting fabric under different working modes.

electrodes connecting to all the core electrodes (Figure 6h22). The gap between the sheath tube and the core column provides the contact-separation motions (Figure 6h21). Different from the above two attached energy-harvesting modes, the sliding mode and freestanding mode rely on the in-plane movements between surface metal electrode and the bottom fabric (Figure 6h31 and 6h41, respectively). A sliding back and forth

between the two will result in a periodical change in electric potential difference, which will drive free electrons to flow alternatively across the electrodes. For the sliding mode, all the sheath electrodes connect with the upper copper electrode (Figure 6h32). However, the freestanding mode consists of two interdigitated sheath electrodes and a freestanding triboelectric layer with grating segments (Figure 6h42). The photographs of

the corresponding load applied methods are also demonstrated in Figure 6i. With the periodic contact separation movements between the triboelectric layer and our energy-harvesting fabric, the real-time OC voltage of corresponding working modes are depicted in Figure 6j. To provide more intuitive comprehension, the four kinds of energy-harvesting modes and their instantaneous electrical output processes are demonstrated in Movie S9 (Supporting Information), from which the flapping frequency can also be well detected. The multimode energy-harvesting fabric shows obvious advantages compared to other energy-harvesting fabrics that only have a single working mode, which will augment the scope for application of wearable energy-harvesting textiles.

As for wearable electronic textiles, washing durability is an essential requirement for their practical long-term usage. In our yarn-based TENG system, with its two ends sealed and all surfaces covered by silicone rubber, which is hydrophobic, washable, and mechanically robust, the whole system is washable and can withstand any kind of complex mechanical agitation. In this work, the washability of the yarn-based TENG is tested with a simulated domestic laundering environment placed on a magnetic stirrer, which includes household detergent and a magnetic stir bar (Figure S20a, Supporting Information). Each laundering cycle lasts 20 min, and the spinning velocity of the magnetic stirrer is controlled at 600 rpm. After running each cycle and drying naturally, the SC current outputs under compressing and stretching states after different washing times are measured (Figure S20b,c, respectively). Furthermore, a long-term cycle result under the compressed state after washing ten times is also presented in Figure S20d in the Supporting Information. The capability to harvest mechanical energy is well maintained without significant decline, clearly indicating its washability as well as robustness and stability. In addition, the power generation stability after being contaminated is also important for energy harvesting textiles. Although the surface contaminations of silicone rubber would decrease the electrical outputs of the yarn-based TENG, its electrical generating capability can be easily recovered as long as the surface contaminations are erased or washed away. Therefore, the surface contaminations have no influence on the long-term usage of the yarn-based TENG.

Owing to the sustainable biomechanical energy harvesting ability and self-powered signal sensing function, the versatile yarn-based TENG has a broad commercial application prospect in self-charging power systems, active sensors, and sustainable energy sources. In addition to the features of light weight, low cost, environmental friendly, and a wide choice of materials, our yarn-based TENG is also machine washable, arbitrary tailorable, and long-term stable, making it more possible to become commercially available device. The combination of the newly TENG technology with traditional textile production makes it more convenient for large-scale production and easier to walk into our daily life. Although some challenges and bottlenecks restrict the practical applications of TENGs, such as yarn's thick diameter, low output power density, low sensing sensitivity, and poor anti-interference ability, effective measures can be taken to solve these problems. For example, the diameter of the TENG-based yarn can be decreased by reducing the amount of silicone rubber coating or adopting coaxial spinning method.

In virtue of structural optimization, material modification, or power management circuit, the output power density of TENG-based energy harvester can be much enhanced. In addition, its lower power output can also be supplemented by integrating with fiber-shaped solar cell and fiber-shaped supercapacitor/lithium ion battery. The sensitivity and anti-interference ability of TENG-based sensors can be improved by adding nanomaterials into its structure and developing matching signal processing system, respectively. With the advantages of excellent performances and high machinability, the wearable yarn-based TENGs are bound to realize large-scale commercial application in the near future.

3. Conclusions

In summary, a multifunctional yarn-based TENG, with the advantages of highly stretchable, flexible, washable, stable and reliable features, is designed and fabricated for versatile and sustainable biomechanical energy harvesting as well as real-time human-interactive sensing. With the silver-coated nylon yarn and silicone rubber as the conductive and dielectric material, respectively, a coaxial core–sheath structure is obtained by inserting an internal core column into an external sheath tube, both of which possess built-in spring-like spiral winding structures. Furthermore, the working mechanism and electrical output performance of the yarn-based TENG are discussed in detail. The inner gap existing in the core–sheath structure provides enough contact and separation space for the internal core column and the external sheath tube. The built-in spiral winding structure endows our yarn-based TENG with high stretchability and meanwhile enables it to quickly respond to diverse mechanical stimuli. At a fixed frequency of 3 Hz, the maximum average power densities of a single yarn-based TENG can reach 11 and 0.88 W m⁻³ under compressing state and stretching state, respectively. Based on the above excellent performances, the yarn-based TENG can be designed as a self-counting skipping rope, a self-powered smart gesture-recognizing glove, and used in a real-time golf scoring system. Furthermore, the yarn-based TENG can be woven into large-area energy-harvesting fabric for more widespread applications, such as lighting up LEDs, charging a commercial capacitor, and driving a digital watch. Moreover, by adjusting the external load imposing method and internal circuit connection mode, we can integrate the four operational modes of TENGs into one piece of fabric together. Our work introduces the core–sheath and built-in spring-like spiral winding structures into the development of multifunctional yarn-based TENGs and verifies their promising applications in both diverse mechanical energy harvesting and real-time self-powered human-interactive sensing.

4. Experimental Section

Preparation of Yarn-Based TENG: For the systematic design of the yarn-based TENG, commercial silver-coated nylon yarn (nominal diameter: 180 μm, resistance <100 Ω cm⁻¹, LessEMF.com) was chosen both as the inner and outer electrodes, and silicone rubber (Ecoflex 0050, Smooth-On, Inc) was selected as the dielectric, supporting, and encapsulating material. First, silicone rubber solution was prepared

by mixing its two components in a 1:1 weight ratio, then blended, and degassed in a vacuum for ≈ 5 min to thoroughly remove bubbles. Second, by syringe injecting the silicone rubber solution into a circular plastic tube, then curing at room temperature (≈ 4 h) and peeling off the plastic tube, a pure silicone rubber fiber column (diameter: 2 mm) was prepared. Third, by spirally winding a silver-coated nylon yarn (inner electrode) on the pure silicone rubber fiber column along its axial direction, an internal core column was obtained. Fourth, an elastic silicone rubber tube, i.e., the middle silicone rubber tube (inner and outer diameter: 3 and 5 mm, respectively, McMaster-Carr) acting as a supporting body was axially and spirally wound with another silver-coated nylon yarn (outer electrode). After encapsulating them with another layer of silicone rubber solution, an external sheath tube was obtained. By inserting the internal core column into the external sheath tube and further sealing their two ends with silicone rubber solution, a yarn-based TENG (average diameter: 6 mm) with built-in spring-like spiral winding and coaxial core–sheath structures was finally fabricated.

Fabrication of Self-Counting Skipping Rope: The self-counting skipping rope mainly consists of three parts: a bottom touchdown section, two middle connection sections, and two hand hold sections. A core conductive yarn, acting as a support skeleton, runs through the bottom and middle sections. In the bottom touchdown section, the core conductive yarn was first covered by a layer of silicone rubber (i.e., the inner silicone rubber layer). After curing, another conductive yarn (i.e., the outer conductive yarn) was spirally wound on the surface of inner silicone rubber layer. In the middle connection section, the outer conductive yarn was directly wound on the core conductive yarn. The architecture of hand hold section was the same as that of the yarn-based TENG. The core conductive yarn from the bottom touchdown and middle connection sections was connected with the outer sheath electrode of the hand hold section. Finally, all the three parts were encapsulated with another silicone rubber layer (i.e., the outer silicone rubber yarn). After curing again, a self-counting skipping rope was obtained.

Fabrication of Large-Area Energy-Harvesting Fabric: The large-area energy-harvesting fabric is easily fabricated into a plain woven pattern with a miniature loom by interlacing regular acrylic yarns (warp yarn) with the parallel-arranged TENG yarns (weft yarn). As for the fabric that can integrate the four operational modes of TENGs together, the regular acrylic yarns and TENG yarns are alternately arranged in the warp direction, and then interwoven with fine polyester yarns from the weft direction.

Methods of Designing Different Working Modes: Through reasonably altering the circuit connection modes and the external load imposing methods, the four operational modes of TENGs can be integrated into one fabric. In the single-electrode mode, all the outer sheath electrodes connected to the ground and a human hand applied a vertical compression load. There was obvious distance existing between human hand and the fabric. In the contact-separation mode, all the core electrodes connected with all the sheath electrodes. A human hand tightly pressed on the fabric and there was almost no gap between them. In the sliding mode, all the outer sheath electrodes connected with the upper copper foil, which acted as the triboelectric layer. In the freestanding mode, the outer sheath electrodes are connected alternatively, and the upper copper foil had a grating structure. The contact and separation movements of the single-electrode and contact-separation modes were applied from the vertical direction (thickness direction), while that of sliding and freestanding modes were imposed from the horizontal direction (in-plane direction).

Finite Element Simulation: The finite element analyses about the potential distribution under open-circuit condition of the yarn-based TENG were conducted by COMSOL software. The inner yarn electrode was connected to the ground, and the surface charge density was applied on the middle silicone rubber tube, which was assumed as -2×10^{-6} C m $^{-2}$. The floating potential was imposed on the outer yarn electrode to balance the potential difference. All the established sizes were based on their actual values.

Washing Test: The experimental simulated washing environment was first cultivated in a beaker with household detergent and a magnetic stir

bar added. Then, a single yarn-based TENG was put directly into the washing solution without any packaging. Then, the as-prepared beaker was placed on a magnetic stirrer to imitate the agitator rotation in a household washing machine. The spinning speed of the magnetic stirrer was set at 600 rpm, and one washing cycle lasted for 20 min. Finally, the yarn-based TENG was rapidly dried in an oven at 60 °C for later electrical output measurement.

Device Characterizations: The surface morphologies of the silver-coated nylon yarn and the internal core column, as well as the cross section of the yarn-based TENG, were characterized by field emission scanning electron microscope (SU-8010, Hitachi). For measuring the electrical output of the yarn-based TENG, various kinds of external force, including compressing, stretching, and bending, were implemented by a commercial linear mechanical motor. The compressing and stretching forces were measured by Vernier LabQuest Mini. The mechanical tensile test was conducted by a universal materials tester (MTS, Model Insight 10). The OC voltage (V_{OC}), SC current (I_{SC}), and SC charge transfer (Q_{SC}) were measured by an electrometer (Keithley 6541 System). The diameter was measured by an electronic digital micrometer (733 Series Electronic Digital Micrometers, L. S. Starrett).

Supporting Information

Supporting Information is available online from the Wiley Online Library or from the author.

Acknowledgements

K.D., J.D., and W.D. contributed equally to this work. The authors are grateful for the supports received from the “Thousands Talents” program for pioneer researcher and his innovation team in China, the Presidential Funding of the Chinese Academy of Science and the National Natural Science Foundation of China (Grant Nos. 51432005, 5151101243, and 51561145021), and Beijing Municipal Science & Technology Commission (Grant No. Z17110000317001). K.D. and J.D. thanks the China Scholarship Council for supporting research at the Georgia Institute of Technology, USA and the fundamental Research Funds for the Central Universities (Grant No. 2232018G-02), China.

Conflict of Interest

The authors declare no conflict of interest.

Keywords

core–sheath structures, human-interactive sensors, mechanical energy harvesting, triboelectric nanogenerator

Received: April 12, 2018

Revised: May 11, 2018

Published online:

- [1] J. A. Rogers, T. Someya, Y. Huang, *Science* **2010**, *327*, 1603.
- [2] W. Zeng, L. Shu, Q. Li, S. Chen, F. Wang, X. M. Tao, *Adv. Mater.* **2014**, *26*, 5310.
- [3] M. Stoppa, A. Chiolerio, *Sensors* **2014**, *14*, 11957.
- [4] M. Kaltenbrunner, G. Adam, E. D. Głowacki, M. Drack, R. Schwödöauer, L. Leonat, D. H. Apaydin, H. Groiss, M. C. Scharber, M. S. White, *Nat. Mater.* **2015**, *14*, 1032.

- [5] Z. Wen, M. H. Yeh, H. Guo, J. Wang, Y. Zi, W. Xu, J. Deng, L. Zhu, X. Wang, C. Hu, L. Zhu, X. Sun, Z. L. Wang, *Sci. Adv.* **2016**, *2*, e1600097.
- [6] A. M. Zamarayeva, A. E. Ostfeld, M. Wang, J. K. Duey, I. Deckman, B. P. Lechêne, G. Davies, D. A. Steingart, A. C. Arias, *Sci. Adv.* **2017**, *3*, e1602051.
- [7] D.-H. Kim, J.-H. Ahn, W. M. Choi, H.-S. Kim, T.-H. Kim, J. Song, Y. Y. Huang, Z. Liu, C. Lu, J. A. Rogers, *Science* **2008**, *320*, 507.
- [8] M. D. Bartlett, E. J. Markvicka, C. Majidi, *Adv. Funct. Mater.* **2016**, *26*, 8496.
- [9] T. Q. Trung, N. E. Lee, *Adv. Mater.* **2016**, *28*, 4338.
- [10] K. Takei, T. Takahashi, J. C. Ho, H. Ko, A. G. Gillies, P. W. Leu, R. S. Fearing, A. Javey, *Nat. Mater.* **2010**, *9*, 821.
- [11] Y. C. Lai, J. Deng, S. Niu, W. Peng, C. Wu, R. Liu, Z. Wen, Z. L. Wang, *Adv. Mater.* **2016**, *28*, 10024.
- [12] M. Kaltenbrunner, T. Sekitani, J. Reeder, T. Yokota, K. Kuribara, T. Tokuhara, M. Drack, R. Schwodiauer, I. Graz, S. Bauer-Gogonea, *Nature* **2013**, *499*, 458.
- [13] D.-H. Kim, N. Lu, R. Ma, Y.-S. Kim, R.-H. Kim, S. Wang, J. Wu, S. M. Won, H. Tao, A. Islam, *Science* **2011**, *333*, 838.
- [14] Y. Wang, L. Wang, T. Yang, X. Li, X. Zang, M. Zhu, K. Wang, D. Wu, H. Zhu, *Adv. Funct. Mater.* **2014**, *24*, 4666.
- [15] A. Koh, D. Kang, Y. Xue, S. Lee, R. M. Pielak, J. Kim, T. Hwang, S. Min, A. Banks, P. Bastien, *Sci. Transl. Med.* **2016**, *8*, 366ra165.
- [16] Z. L. Wang, *Adv. Mater.* **2012**, *24*, 280.
- [17] Z. L. Wang, *Faraday Discuss.* **2015**, *176*, 447.
- [18] Z. L. Wang, *ACS Nano* **2013**, *7*, 9533.
- [19] B. S. Shim, W. Chen, C. Doty, C. Xu, N. A. Kotov, *Nano Lett.* **2008**, *8*, 4151.
- [20] D. S. Hecht, L. Hu, G. Irvin, *Adv. Mater.* **2011**, *23*, 1482.
- [21] Y. Meng, Y. Zhao, C. Hu, H. Cheng, Y. Hu, Z. Zhang, G. Shi, L. Qu, *Adv. Mater.* **2013**, *25*, 2326.
- [22] I. Khrapach, F. Withers, T. H. Bointon, D. K. Polyushkin, W. L. Barnes, S. Russo, M. F. Craciun, *Adv. Mater.* **2012**, *24*, 2844.
- [23] H. Wu, D. Kong, Z. Ruan, P.-C. Hsu, S. Wang, Z. Yu, T. J. Carney, L. Hu, S. Fan, Y. Cui, *Nat. Nanotechnol.* **2013**, *8*, 421.
- [24] L. Hu, G. Zheng, J. Yao, N. Liu, B. Weil, M. Eskilsson, E. Karabulut, Z. Ruan, S. Fan, J. T. Bloking, M. D. McGehee, L. Wagberg, Y. Cui, *Energy Environ. Sci.* **2013**, *6*, 513.
- [25] M. Vosgueritchian, D. J. Lipomi, Z. Bao, *Adv. Funct. Mater.* **2012**, *22*, 421.
- [26] S. Wang, L. Lin, Z. L. Wang, *Nano Energy* **2015**, *11*, 436.
- [27] G. Zhu, W. Q. Yang, T. Zhang, Q. Jing, J. Chen, Y. S. Zhou, P. Bai, Z. L. Wang, *Nano Lett.* **2014**, *14*, 3208.
- [28] Z. L. Wang, J. Chen, L. Lin, *Energy Environ. Sci.* **2015**, *8*, 2250.
- [29] Z. L. Wang, L. Lin, J. Chen, S. Niu, Y. Zi, *Triboelectric Nanogenerators*, Springer International Publishing, Heidelberg, Germany **2016**.
- [30] Z. L. Wang, *Mater. Today* **2017**, *20*, 74.
- [31] K. Dong, J. Deng, Y. Zi, Y. C. Wang, C. Xu, H. Zou, W. Ding, Y. Dai, B. Gu, B. Sun, Z. L. Wang, *Adv. Mater.* **2017**, *29*, 1702648.
- [32] X. Wen, W. Yang, Q. Jing, Z. L. Wang, *ACS Nano* **2014**, *8*, 7405.
- [33] J. Chen, Z. L. Wang, *Joule* **2017**, *1*, 480.
- [34] Y. Yang, G. Zhu, H. Zhang, J. Chen, X. Zhong, Z.-H. Lin, Y. Su, P. Bai, X. Wen, Z. L. Wang, *ACS Nano* **2013**, *7*, 9461.
- [35] J. Xiong, M.-F. Lin, J. Wang, S. L. Gaw, K. Parida, P. S. Lee, *Adv. Energy Mater.* **2017**, *7*, 1701243.
- [36] Q. Jing, Y. Xie, G. Zhu, R. P. Han, Z. L. Wang, *Nat. Commun.* **2015**, *6*, 8031.
- [37] Z. Liu, S. Fang, F. Moura, J. Ding, N. Jiang, J. Di, M. Zhang, X. Lepró, D. Galvão, C. Haines, *Science* **2015**, *349*, 400.
- [38] S. H. Kim, C. S. Haines, N. Li, K. J. Kim, T. J. Mun, C. Choi, J. Di, Y. J. Oh, J. P. Oviedo, J. Bykova, *Science* **2017**, *357*, 773.
- [39] K. Dong, Y.-C. Wang, J. Deng, Y. Dai, S. L. Zhang, H. Zou, B. Gu, B. Sun, Z. L. Wang, *ACS Nano* **2017**, *11*, 9490.
- [40] S. Niu, Z. L. Wang, *Nano Energy* **2015**, *14*, 161.